

Topological Superconductor $\text{Bi}_2\text{Te}_3/\text{NbSe}_2$ heterostructures

Jin-Peng Xu^{1†}, Canhua Liu^{1†}, Mei-Xiao Wang¹, Jianfeng Ge¹, Zhi-Long Liu¹, Xiaojun Yang², Yan Chen³, Ying Liu^{1,4}, Zhu-An Xu², Chun-Lei Gao¹, Dong Qian¹, Fu-Chun Zhang^{2,5}, Qi-Kun Xue⁶, and Jin-Feng Jia^{1*}

¹Key Laboratory of Artificial Structures and Quantum Control (Ministry of Education), Department of Physics and Astronomy, Shanghai Jiao Tong University, Shanghai 200240, China

²State Key Laboratory of Silicon Materials and Department of Physics, Zhejiang University, Hangzhou 310027, China

³Department of Physics, Fudan University, Shanghai 200433, China

⁴Department of Physics, Pennsylvania State University, University Park, PA 16802, USA

⁵Department of Physics, Hong Kong University, Hong Kong, China

⁶State Key Laboratory for Low-Dimensional Quantum Physics, Department of Physics, Tsinghua University, Beijing 100084, China

Topological superconductors (TSCs) have a full gap in the bulk and gapless surface states consisting of Majorana fermions, which have potential applications in fault-tolerant topological quantum computation. Because TSCs are very rare in nature, an alternative way to study the TSC is to artificially introduce superconductivity into the surface states of a topological insulator (TI) through proximity effect (PE)¹⁻⁴. Here we report the first experimental realization of the PE induced TSC in $\text{Bi}_2\text{Te}_3/\text{NbSe}_2$ thin films as demonstrated by the density of states probed using scanning tunneling microscope. We observe Abrikosov vortices and lower energy bound states on the surface of topological insulator and the dependence of superconducting coherence length on the film thickness and magnetic field, which are attributed to the superconductivity in the topological surface states. This work demonstrates the practical feasibility of fabricating a TSC with individual Majorana fermions inside superconducting vortex as predicted in theory and accomplishes the pre-requisite step towards searching for Majorana fermions in the PE induced TSCs.

† J.P.X. and C. L. contributed equally to this work.

* Corresponding author: jfjia@sjtu.edu.cn.

When a normal metal (NM) and a superconductor (SC) are brought into contact, Cooper pairs will be introduced into the NM through the interface, resulting in a superconducting energy gap at the Fermi level (E_F) in NM. This phenomenon is called the superconducting PE⁵. Since the pairing symmetry of the PE induced Cooper pairs is determined by the electronic structures of the NM, TSCs that have p-wave-like pairing symmetry as well as time reversal symmetry can be obtained by the combination of a simple s-wave SC and a NM with a peculiar band structure that requires an odd number of spin non-degenerate electronic bands crossing E_F ^{3,4}. TSCs are predicted to host Majorana fermions and thus attract a great deal of research interest. For example, a semiconductor nanowire with strong spin-orbit coupling fabricated on an s-wave SC may realize bound Majorana fermions located at the wire's two ends in an external magnetic field^{6,7}. Another proposed material for the construction of a TSC is a three dimensional TI that has a spin textured topological surface state band located in the bulk energy gap^{8,9}. Fu and Kane predicted that when Cooper pairs are introduced to its topological surface states via PE, the surface of the TI will turn into a TSC that can harbor Majorana fermions bound at Abrikosov vortex cores².

Recently, PE induced superconductivity in surface states of a TI has been manifested in electronic transport measurement on several TI/SC heterostructures¹⁰⁻¹⁴, but the pairing symmetry has not been clarified in experiment yet. While an indirect signature of Majorana fermions was revealed in a Josephson current measurement performed on an Al/Bi₂Se₃/Al junction¹², more explicit evidence for the TSC with Majorana fermions can be obtained by direct detection of zero-energy bound states at Abrikosov vortex cores in a TI/SC heterostructure. Although Abrikosov vortices on ordinary SCs have been widely demonstrated in experiments¹⁵⁻¹⁷, they are yet to be observed in a PE-induced SC, mainly due to the difficulty in preparing an atomically smooth interface and surface of the NM/SC heterostructure. In our previous work, we succeeded in constructing a TI/SC heterostructure by growing a Bi₂Se₃ thin film on a NbSe₂ single crystal, where the coexistence of Cooper pairs and

topological surface states was demonstrated¹⁸. In this work, we report observation of PE superconductivity on another TI/SC heterostructure, $\text{Bi}_2\text{Te}_3/\text{NbSe}_2$, using scanning tunnelling microscopy/spectroscopy (STM/S) by greatly improving the film quality. We have systematically studied multi quantum-layers (QL) of Bi_2Te_3 on top of NbSe_2 . When the Fermi level is within the bulk gap, the superconducting tunnelling spectra of the $\text{Bi}_2\text{Te}_3/\text{NbSe}_2$ surface deviate from the usual s-wave spectra, indicating PE superconductivity on the surface. We have succeeded in observing Abrikosov vortices and bound states inside the vortex core, in which a zero-bias bound state, or Majorana fermion has been predicted in theory. These experimental results provide the evidence for PE induced topological superconducting states on the surfaces of the TI films, which paves the way for detecting Majorana fermions -or even an individual Majorana fermion - on a TI/SC heterostructure.

The growth mode of Bi_2Te_3 is the same as that of Bi_2Se_3 on NbSe_2 ¹⁸, i.e., layer by layer growth as shown in Figs. 1(a)-1(b). The excellent crystallization of the Bi_2Te_3 film is seen in its STM image with an atomic resolution. Due to its higher growth temperature, the Bi_2Te_3 film has very large terraces that are crucial for observing vortices in this work. The Bi_2Te_3 film is not interfaced with the NbSe_2 substrate directly but separated by a Bi layer in between, so that the first quintuple layer (QL) of Bi_2Te_3 has a step height of 1.6nm in STM images. All other QLs have the thickness of 1.0nm, similar to those grown on a Si(111) substrate¹⁹. Previous studies found that the topological surface state of a Bi_2Te_3 thin film grown on Si(111) does not form a Dirac cone until the thickness reaches 2 to 4QL because of the hybridization between the top and bottom surface states of the film²⁰⁻²². Once the Dirac cone forms, the band structure near the Fermi energy does not change dramatically except for a rigid energy shift with increasing the thickness of the Bi_2Te_3 film. On the NbSe_2 substrate, we also observed a similar evolution of the electronic states in STS data with the increase of Bi_2Te_3 thickness, as shown in Fig. 1(c). The differential conductance curve (dI/dV spectrum) taken with STS, obtained on a 20QL Bi_2Te_3 film grown on a Si(111) surface has a deformed U-shape segment in the energy range between the bulk valence band maximum (VBM) and the

conduction band minimum (CBM), as indicated by blue and red arrows in Fig. 1(c), respectively. Similar deformed U-shape segments are also seen in dI/dV spectra taken on $\text{Bi}_2\text{Te}_3/\text{NbSe}_2$ at thicknesses of no less than 3QL. With the increase of Bi_2Te_3 thickness, the deformed U-shape segment shifts to higher binding energy while keeping its size in energy scale. This indicates that the topological surface states on $\text{Bi}_2\text{Te}_3/\text{NbSe}_2$ come into existence at a thickness of 3QL, very similar behavior to that of Bi_2Te_3 films grown on Si(111) substrates²⁰.

The superconducting energy gap was observed on the Bi_2Te_3 thin films in STS data. Fig. 2(a) is a series of dI/dV spectra taken on $\text{Bi}_2\text{Te}_3/\text{NbSe}_2$ at 0.4K, showing strong thickness dependence. Fig. 2(b) presents the dI/dV spectra of bare NbSe_2 , 2QL, and 3QL Bi_2Te_3 films. Up to a thickness of 2QL, the STS curve has a flat bottom that touches the zero value of the differential conductance at around zero bias. The STS curve can be well fitted by an s-wave BCS-type spectrum function [Fig. 2(b)-bottom and middle]. In contrast, the spectra of Bi_2Te_3 films of more than 2QL have a non-flat bottom that does not touch the zero of the differential conductance. Clearly, an s-wave BCS-type spectral function can no longer fit the spectrum of a 3QL Bi_2Te_3 film [Fig. 2(b)-top]. A simple s-wave BCS-like fitting curve can neither reproduce the spectrum near zero-bias, nor the sharp coherence peak near the position of the energy gap. The differences could be induced by PE, where pair field diminished into the films, therefore the coherence length increases, and also the quasiparticle lifetime increases so that states appear at bottom of gap. However, the similar behavior was not observed on 1 or 2QL films, and abruptly became obvious on 3QL films, where the topological surface states form. So, the formation of topological surface states might play some role for the deviation of the 3QL's dI/dV spectrum from s-wave BCS-like behavior^{23, 24}. Note that a simple p-wave like pairing for topological superconductor gives essentially the same dI/dV spectra as s-wave BCS at the relevant energy region.

The data up to 11QL are fitted by thermally broadened s-wave BCS-like curves²⁵, and the results are summarized in

Fig. 2(c). Roughly speaking, the gap value decreases exponentially as the thickness increases, qualitatively consistent with the energy gap decay for PE-induced superconductivity. However, a kink can obviously be seen at 6QL, where the Fermi level is already in the bulk band gap [see Fig.1(c)]. The unusual character implies two-band superconducting, i.e., bulk superconducting state and surface superconducting state. At 6QL or more, surface superconducting state may dominate, so the superconducting gap decays slower.

Since the formation of the small energy gap at the Fermi level is due to quasi particle excitations in a superconductor, the dI/dV spectra measured on $\text{Bi}_2\text{Te}_3/\text{NbSe}_2$ should also have strong dependence on external magnetic fields, which suppress the formation of Cooper pairs. In Fig. 3(a), we show a series of spatially averaged dI/dV spectra taken on a 3QL $\text{Bi}_2\text{Te}_3/\text{NbSe}_2$ sample at various perpendicular magnetic fields. With the increase of the magnetic field, the energy gap becomes smaller and gap feature near the zero bias in the dI/dV spectra becomes shallower. The energy gap disappears at about 2.4T, which is substantially smaller than the upper (perpendicular) critical field H_{c2} (3.2 T) of the NbSe_2 substrate.

Large terraces of the $\text{Bi}_2\text{Te}_3/\text{NbSe}_2$ surface make it possible to image Abrikosov vortices with STS²⁶. Figs. 3(b)-3(c) show dI/dV maps at zero bias, i.e., the contour of zero bias conductance (ZBC), recorded on a 3QL $\text{Bi}_2\text{Te}_3/\text{NbSe}_2$ and bare NbSe_2 surfaces under perpendicular magnetic fields. It is seen from Fig. 3(c) that the vortices exhibit a highly ordered hexagonal lattice just like those observed on the clean NbSe_2 surface shown in Fig. 3(b). This is the first time the vortex has been clearly observed in a proximity induced topological superconductor. Due to the crystalline band structure and the interaction of the neighboring vortices in the hexagonal lattice, a six-fold symmetry is explicitly observed in the vortex images of the bare NbSe_2 surface [Fig. 3(d)]. The same symmetry is also present on the ZBC contour of the 5QL Bi_2Te_3 film [Fig. 3(e)]. The growth of Bi_2Te_3 films on NbSe_2 does not change the orientation of the vortex lattice to avoid extra energy consumption for magnetic flux penetrating the

Bi₂Te₃/NbSe₂ samples. This may be seen with the aid of the two hexagons superimposed on Figs. 3(d) and 3(e) (dashed lines). Also, from the size of the unit cell of the vortex lattice, we can calculate the magnetic flux penetrating through one vortex cylinder. The obtained value is very close to a magnetic flux quantum, i.e., $\Phi_0 = h/2e$, in which h is Planck's constant and e is the electric charge of an electron.

By carefully comparing the vortices obtained on NbSe₂ and 3QL Bi₂Te₃ shown in Figs. 3(b) and 3(c), respectively, one can see that the vortex size is a little smaller on NbSe₂ than that on 3QL Bi₂Te₃. We investigated the spatial extension of the vortex for different Bi₂Te₃ thickness. The ZBC line-profile crossing through the center of the vortex can be very well fitted by the formula below, derived from the Ginzburg-Landau (GL) expression for the superconducting order parameter¹⁷:

$$\sigma(r, 0) = \sigma_0 + (1 - \sigma_0) \times \{1 - \tanh[r/(\sqrt{2}\xi)]\}, \quad (1)$$

where σ_0 is the normalized ZBC away from a vortex core, r is the distance to the vortex center and ξ is the GL coherence length in plane. The experimental data and fitted results for bare NbSe₂ and 3QL Bi₂Te₃/NbSe₂ are shown in Figs. 4(a), giving $\xi_{NbSe_2}=16\text{nm}$ and $\xi_{3QL}=29\text{nm}$ at 0.4K and 0.1T. Similar analyses were also performed on other samples, finding a monotonic increase of coherence length with Bi₂Te₃ thickness as shown in Fig. 4(b). This is consistent with the above result that H_{c2} of 3QL Bi₂Te₃/NbSe₂ is smaller than that of bare NbSe₂, since a larger ξ gives a smaller H_{c2} according to the GL expression, $H_{c2} = \Phi_0/(2\pi\xi^2)$.

As the in-plane ξ of a NbSe₂ single crystal varies from 7.2nm to 28.2nm in previous reports^{27, 28}, ξ obtained above for the bare NbSe₂ is a reasonable value. For Bi₂Te₃ films, the Pippard's coherence length can be estimated to be about 116nm by the formula $\xi_0 = hv_F/(\pi^2\Delta)$, in which v_F is the Fermi velocity, previously reported to be $3.32 \times 10^5 \text{m/s}$ ²⁴. In the dirty limit, which is the case for the NbSe₂ substrate and thus should be also for the proximity induced TI/SC heterostructure, $\xi = \xi_0$ at T=0 K. The discrepancy between the estimation and the above

experimental results lies in the fact that the Bi_2Te_3 film is a PE-induced superconductor, and the properties of the induced Cooper pairs are inevitably influenced by the parent superconductor of NbSe_2 . As the thickness of the Bi_2Te_3 film increases, the influence from the NbSe_2 substrate on the Bi_2Te_3 film becomes weaker, resulting in a longer coherence length.

Variation of magnetic field leads to changes of the vortex size and the coherence length. The magnetic field dependence of the coherence length is shown in Fig. 4(c) for 5QL $\text{Bi}_2\text{Te}_3/\text{NbSe}_2$. As magnetic field increases, the coherence length decreases initially and then saturates at magnetic field reaches about 0.7T. For a single band s-wave superconductor, the vortex size or the coherence length is insensitive to the magnetic field at the weak field. The strong dependence of the vortex size with the field is a clear evidence of non-single band s-wave nature for the vortex state and is consistent with the scenario that both the bulk conduction and surface states are superconducting and contributing to the vortex state. In brief, all the facts in our experiment demonstrate the topological surface states on $\text{Bi}_2\text{Te}_3/\text{NbSe}_2$ are superconducting and $\text{Bi}_2\text{Te}_3/\text{NbSe}_2$ is a topological superconductor, which can host the Majorana fermions in the vortex core. It is noted that the superconductivity in topological surface states has been confirmed recently by ARPES²⁹.

Majorana mode is the zero-energy bound state in the vortex core, and the first step to detect it is to observe the peak caused by the bound states in the vortex core. The bound-state peaks were observed in 1-6QL $\text{Bi}_2\text{Te}_3/\text{NbSe}_2$ as shown in Fig. 4(d). However, these peaks contain all bound states near the Fermi energy, could not be identified as a signature of Majorana fermions. Actually, the peaks are also observed on bare NbSe_2 and 1-2QL Bi_2Te_3 films, and their heights are even higher than those of 3-6QL Bi_2Te_3 films. The bound states occur at energies where constructive interference of multiply reflected electron-like and hole-like states forms. In a 2D chiral p-wave SC, the energy separation of the bound states is theoretically predicted to be $\delta E = \Delta_0^2/E_F$ ³⁰, which is the minigap

protecting the zero-energy Majorana fermion excitations from thermal effects. In recent theoretical work³¹, the minigap of a PE-induced TSC is evaluated by $\delta E \approx 0.83\Delta_0^2 / \sqrt{\Delta_0^2 + E_F^2}$. In order to increase the robustness of Majorana fermions to thermal effect and to resolve them with STS, one needs to decrease the sample temperature as much as possible and increase δE by shifting E_F towards the Dirac point. For a 5QL $\text{Bi}_2\text{Te}_3/\text{NbSe}_2$ sample, for example, at a temperature of 300mK that corresponds to a thermal energy of 0.026meV, if E_F can be shifted to within 5meV of the Dirac point, the δE will be about 0.1meV, which is much larger than the thermo energy and can be resolved by STS. The E_F can be tuned by doping, or alloying Sb_2Te_3 and Bi_2Te_3 ³², etc., However, chemical doping or engineering will reduce the sample quality and thus requires a much greater experimental efforts to achieve the precise control of the Fermi level, and tuning E_F in the gap also suppresses the PE, resulting a smaller T_c , which makes the experiment more challenging.

In summary, we have provided experimental evidences for the superconductivity in topological surface states induced by PE. Our work confirms the theoretical prediction that TSC can be realized in a TI/SC heterostructure. Abrikosov vortex lattices and bound states at the vortex cores have been successfully observed for the first time on the PE induced artificial topological superconducting $\text{Bi}_2\text{Te}_3/\text{NbSe}_2$ heterostructure. Our study is an important step in search predicted Majorana fermions inside the vortex core of TSC.

Methods

All experiments were performed in situ on a commercial apparatus with base pressures of 3×10^{-10} torr for sample growth and 7×10^{-11} torr for STM measurement. NbSe_2 crystal was cleaved at room temperature in UHV after sufficient degassing at 250°C. Te and Bi atoms were co-deposited onto the NbSe_2 surface at 250°C. 5 minutes post annealing was conducted to eliminate excess Te atoms in the Bi_2Te_3 films. All prepared samples were transferred to a cooling stage kept at 4.2K for STM measurement, in which electrochemically etched tungsten tips were used

after heating and silver-decoration in situ. A lower sample temperature of 0.4K was achieved by using liquid ^3He . To obtain dI/dV spectra at a given location, the tip-sample separation was held constant and a lock-in amplifier was used to modulate the bias voltage by dV (0.15mV or 3mV depending on the spectral range of interest) with a frequency of 991Hz. The vortex image is the record of each pixel's ZBC while bias voltage is ramped from 0.05mV to 0V with feedback off.

Acknowledgements

This work was supported by the National Basic Research Program of China (Grant No. 2012CB927401, 2011CB921902, 2013CB921902, 2011CB922200, 2012CB921604), NSFC (Grant No. 91021002, 11174199, 11134008, 11274228, 11074043, 11274269), Shanghai Committee of Science and Technology, China (No. 11JC1405000, 11PJ1405200, 12JC1405300), Shanghai Municipal Education Commission (11ZZ17).

Reference

- [1] Qi, X. L. *et al.* Time-Reversal-Invariant Topological Superconductors and Superfluids in Two and Three Dimensions. *Phys. Rev. Lett.* **102**, 187001 (2009).
- [2] Fu, L. & Kane, C. Superconducting Proximity Effect and Majorana Fermions at the Surface of a Topological Insulator. *Phys. Rev. Lett.* **100**, 096407 (2008).
- [3] Alicea, J. New directions in the pursuit of Majorana fermions in solid state systems. *Rep. Prog. Phys.* **75**, 076501 (2012).
- [4] Beenakker, C. W. J. Search for Majorana fermions in superconductors. *Annu. Rev. Con. Mat. Phys.* **4**, 113 (2013).
- [5] Kim, J. *et al.* Visualization of geometric influences on proximity effects in heterogeneous superconductor thin films. *Nature Phys.* **8**, 464-469 (2012).
- [6] Mourik V. *et al.* Signatures of Majorana Fermions in Hybrid Superconductor-Semiconductor Nanowire Devices. *Science* **336**, 6084 (2012).
- [7] Lutchyn, R. M. *et al.* Majorana Fermions and a Topological Phase Transition in Semiconductor-Superconductor Heterostructures. *Phys. Rev. Lett.* **105**, 077001 (2010).
- [8] Hasan, M. Z. & Kane, C. L. Topological insulators. *Rev. Mod. Phys.* **82**, 3045-3067 (2010).
- [9] D. Hsieh *et al.* A topological Dirac insulator in a quantum spin Hall phase. *Nature* **452**, 970-974 (2008).
- [10] Williams, J. R. *et al.* Unconventional Josephson Effect in Hybrid Superconductor-Topological Insulator Devices. *Phys. Rev. Lett.* **109**, 056803 (2012).
- [11] Benjamin, S. *et al.* Gate-tuned normal and superconducting transport at the surface of a topological insulator. *Nature Commun.* **2**, 575 (2011).
- [12] Veldhorst, *et al.* Josephson Supercurrent through a Topological Insulator Surface State. *Nature Mater.* **11** 417 (2012);
- [13] Qu, F. M. *et al.* Strong Superconducting Proximity Effect in Pb-Bi₂Te₃ Hybrid Structures. *Sci. Rep.* **2**, 339 (2012).
- [14] Zareapour, P. *et al.* Proximity-induced high-temperature superconductivity in the topological insulators Bi₂Se₃ and Bi₂Te₃. *Nature Commun.* **3**, 1056 (2012).
- [15] Guillamón, I. *et al.* Direct observation of melting in a two-dimensional superconducting vortex lattice. *Nature Phys.* **5**, 651-655 (2009).
- [16] Fischer, Ø. *et al.* Scanning tunneling spectroscopy of high-temperature superconductors. *Rev. Mod. Phys.* **79**, 353 (2007).
- [17] Eskildsen, M. R. *et al.* Vortex Imaging in the π Band of Magnesium Diboride. *Phys. Rev. Lett.* **89**, 187003 (2002).
- [18] Wang, M. X. *et al.* The Coexistence of Superconductivity and Topological Order in the Bi₂Se₃ Thin Films. *Science* **336**, 52-55 (2012).
- [19] Chen, X. *et al.* Molecular Beam Epitaxial Growth of Topological Insulators. *Adv. Mater.* **23**, 1162-1165 (2011).
- [20] Li, Y. Y. *et al.* Intrinsic Topological Insulator Bi₂Te₃ Thin Films on Si and Their Thickness Limit. *Adv. Mater.* **22**, 4002 (2010).
- [21] Park, K. *et al.* Robustness of Topologically Protected Surface States in Layering of Bi₂Te₃ Thin Films. *Phys. Rev. Lett.* **105**, 186801 (2010).
- [22] Liu, Y. *et al.* Topological limit of ultrathin quasi-free-standing Bi₂Te₃ films grown on Si(111). *Phys. Rev. B* **85**, 195442 (2012).
- [23] Black-Schaffer, A. M. & Balatsky, A. V. Proximity-induced unconventional superconductivity in topological insulators. *Phys. Rev. B* **87**, 220506(R) (2013).
- [24] Tkachov, G. Suppression of surface p-wave superconductivity in disordered topological insulators. arXiv: 1304.0631 (2013).
- [25] Dynes, R. C. *et al.* Direct Measurement of Quasiparticle-Lifetime Broadening in a Strong-Coupled Superconductor. *Phys. Rev. Lett.* **41**, 1509 (1978).
- [26] Hess, H. F. *et al.* Scanning-Tunneling-Microscope Observation of the Abrikosov Flux Lattice and the Density of

- States near and inside a Fluxoid. *Phys. Rev. Lett.* **62**, 214-216 (1989).
- [27] Sonier, J. E. *et al.* Muon-Spin Rotation Measurements of the Magnetic Field Dependence of the Vortex-Core Radius and Magnetic Penetration Depth in NbSe₂. *Phys. Rev. Lett.* **79**, 1742 (1997).
- [28] Miller, R. I. *et al.* Low Temperature Limit of the Vortex Core Radius and the Kramer-Pesch Effect in NbSe₂. *Phys. Rev. Lett.* **85**, 1540-1543 (2000).
- [29] Wang, E. *et al.* Fully gapped topological surface states in Bi₂Se₃ films induced by a d-wave high-temperature superconductor. *Nature Phys.* **9**, 621 (2013).
- [30] Caroli, C. *et al.* Bound Fermion states on a vortex line in a type II superconductor. *Phys. Lett.* **9**, 307-309 (1964).
- [31] Sau, J. D. *et al.* Robustness of Majorana fermions in proximity-induced superconductors. *Phys. Rev. B* **82**, 094522 (2010).
- [32] Zhang, J. *et al.* Band structure engineering in Bi_{2-x}Sb_xTe₃ topological insulators. *Nature Commun.* **2**, 574 (2011).

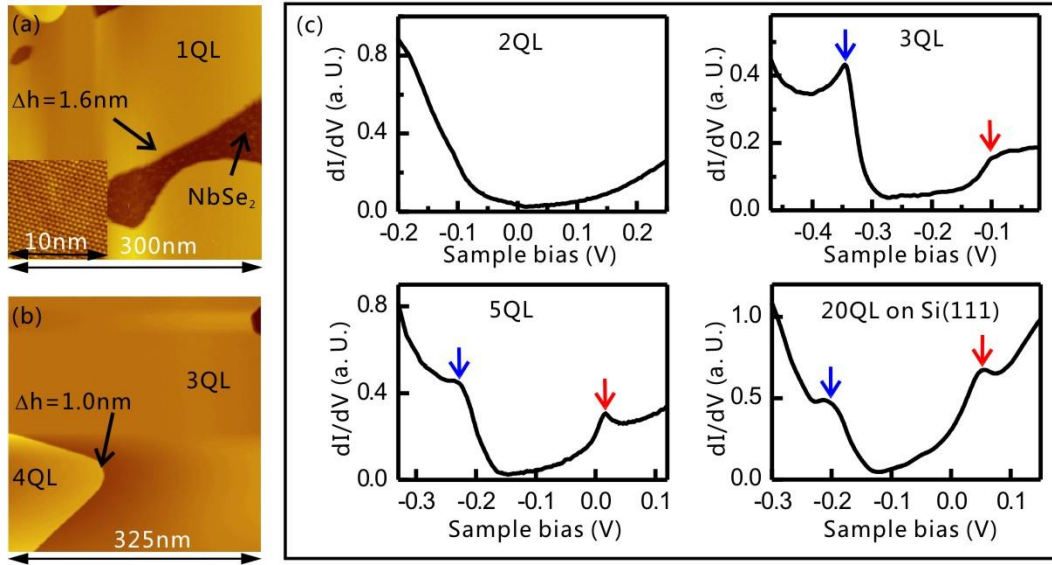


Fig. 1. Morphology and electronic density of states of Bi₂Te₃ thin films of different coverages, grown on a NbSe₂ substrate. (a) and (b) Large-scale STM images of Bi₂Te₃ thin films. The insert in (a) shows the atomic resolution of the Bi₂Te₃ surface taken on a 3QL terrace. (c) dI/dV spectra measured at 4.2K on 2QL, 3QL and 5QL Bi₂Te₃/NbSe₂ heterostructures and on a 20QL Bi₂Te₃ film grown on a Si(111) surface. Blue and Red arrows indicate the energy position of VBM and CBM, respectively.

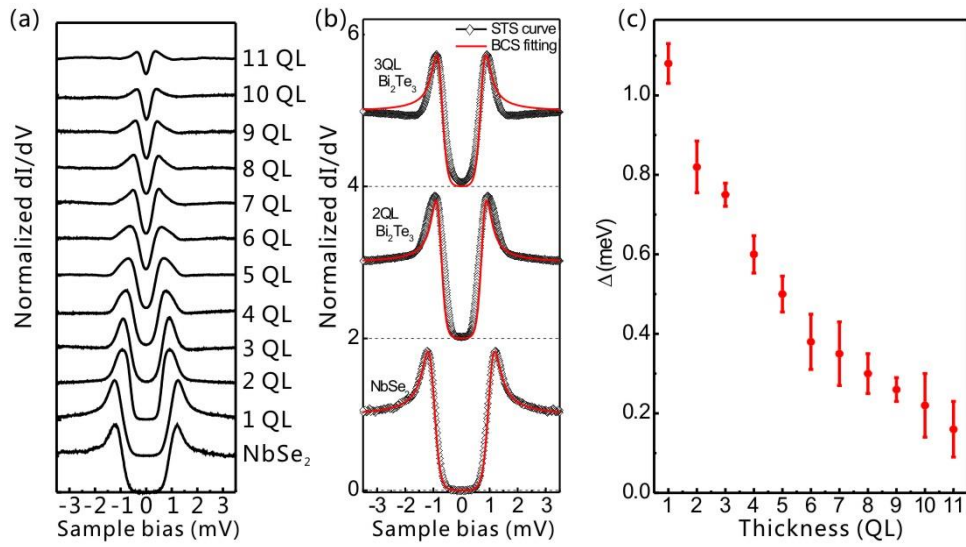


Fig. 2. Superconducting energy gap observed on Bi₂Te₃/NbSe₂. (a) A series of dI/dV spectra taken on different thicknesses of Bi₂Te₃ thin films at 0.4K. (b) dI/dV spectra measured at 0.4K of bare NbSe₂, and 2QL and 3QL of Bi₂Te₃ thin films all superimposed with standard BCS-like fitting results. The latter two spectra are shifted upward by 2 and 4, respectively. (c) Thickness dependence of the energy gap obtained from the BCS-like fitting.

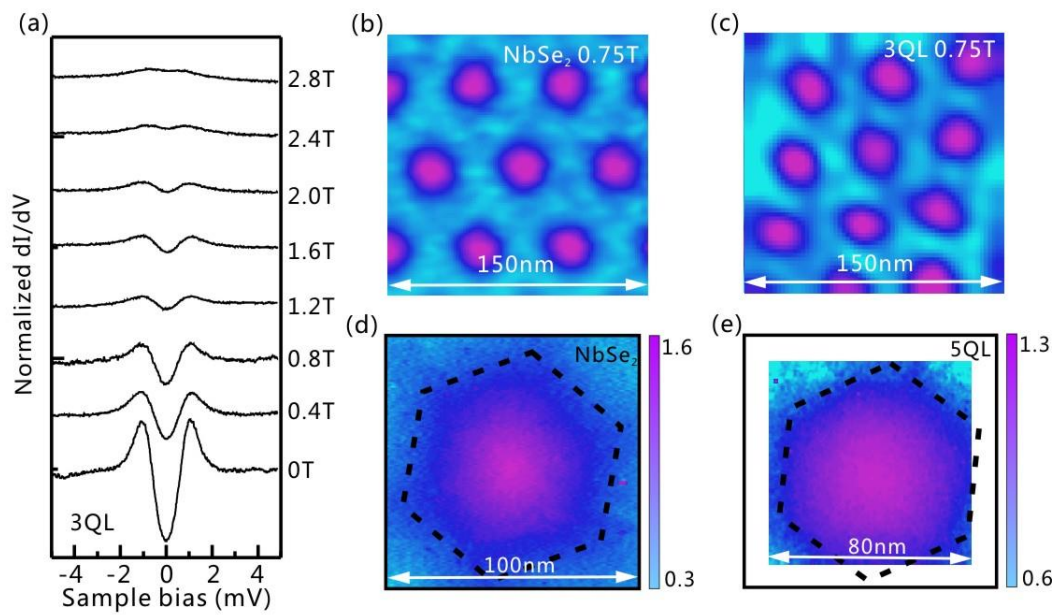


Fig. 3 (a) Dependence of dI/dV spectra on magnetic field measured on a 3QL Bi_2Te_3 thin film at 0.4K. (b) and (c) Zero bias dI/dV maps measured at 0.4K and 0.75T for NbSe_2 and 3QL $\text{Bi}_2\text{Te}_3/\text{NbSe}_2$ heterostructures. (d) and (e) Zero bias dI/dV maps for a single vortex measured at 0.4K and 0.1T on NbSe_2 and 5QL $\text{Bi}_2\text{Te}_3/\text{NbSe}_2$. The superimposed hexagons in dashed lines indicate the shape of the vortices.

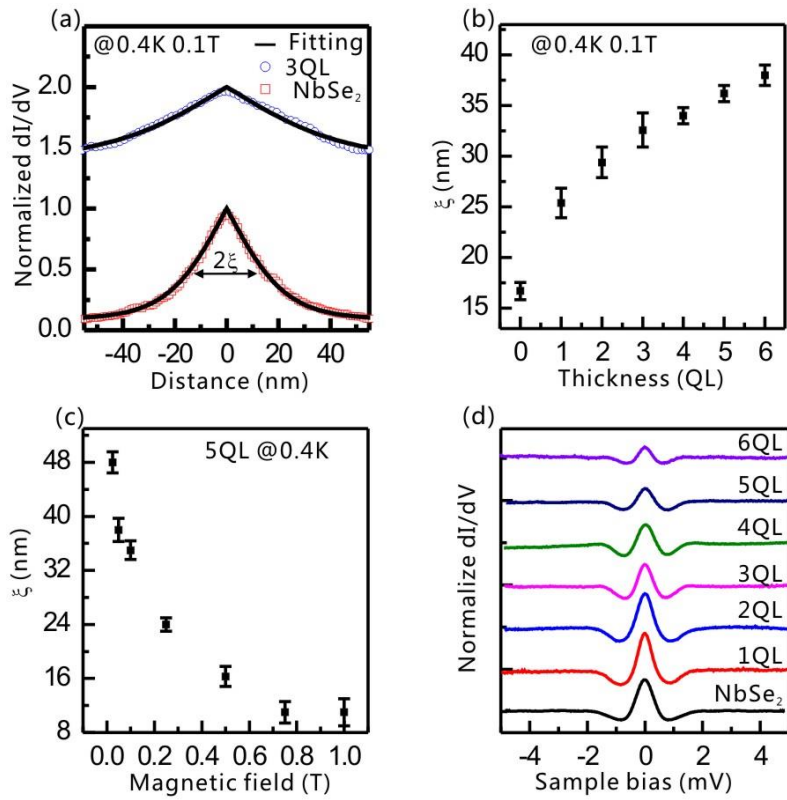


Fig. 4 (a) Normalized ZBC profiles crossing through the centers of vortices at 0.4K and 0.1T on NbSe₂ and 3QL Bi₂Te₃, respectively. The superimposed lines are fitted results using Eq. (1). The 3QL data is shifted upward by 1.5 for a better view. The obtained coherence length as a function of thickness is summarized in (b). (c) The coherence length as a function of magnetic field measured on 5QL Bi₂Te₃/NbSe₂. (d) Thickness dependence of dI/dV spectra measured at centers of vortices on NbSe₂ and 1-6QL Bi₂Te₃/NbSe₂ at 0.4 K.